Optics & Laser Technology 168 (2024) 109992

Contents lists available at ScienceDirect

Optics and Laser Technology

journal homepage: www.elsevier.com/locate/optlastec

Full length article

Optical properties of tilted surfaces in material jetting

Ali Payami Golhin *, Are Strandlie

Department of Manufacturing and Civil Engineering, NTNU - Norwegian University of Science and Technology, Gjøvik 2815, Norway

ARTICLE INFO

Keywords:
Material jetting
Digital materials
Spectral analysis
Appearance measurement
Principal component analysis

ABSTRACT

Material jetting (MJT) is a promising additive manufacturing (AM) technique that offers high-quality appearance reproduction. Considering the limited selection of aesthetic materials available for MJT technology, a thorough optical analysis is required to determine their optimal application. This study focuses on the prominent appearance attributes in MJT and the role of texture variation due to different build orientations (BOs). For this purpose, tilted surfaces were manufactured in a direction ranging from 0° to 90° degrees at 15° intervals. The spectral reflectance, absorbance, transmittance, color difference, gloss, haze, scattering, and texture of MJT objects with varying BOs were investigated. To illustrate the variation in visual appearance and texture of the studied surfaces, the optical properties were rendered to three-dimensional (3D) spherical models. Further, the interaction of the appearance of 3D printing interacts with the quality improvement of AM surfaces is discussed. The results indicated that BO significantly affected the surface texture and layer orientation, leading to variation in surface quality by impacting all studied appearance attributes. Furthermore, tilted MJT surfaces exhibited more variation in reflectance than transmittance. As a result of the Kendall rank correlation coefficient and principal component analysis (PCA), light transmittance through parts manufactured at BO 75° showed the largest variation compared to 0°. Regarding light reflectance, 60° showed more variation among studied angles. The results of gloss, haze, and scattering studies revealed the significance of the measurement direction due to the role of microsurface normals in the surface texture.

1. Introduction

Rapid prototyping converts digital models to physical inventory. Prototyping allows for identifying new opportunities for continued exploration of an unexplored space of designs [1]. High-detail prototyping has been the primary goal of AM technologies for many years, and it still drives the sales of most 3D printers [2]. Prototyping efficiency can be enhanced by improving the surface quality of as-printed objects, both for short-term [3] and long-term [4] applications. As a result of full-color 3D printing (3DP) equipment, including material jetting (MJT) systems, the expectation for photorealistic and complex prototypes is increasing. Nevertheless, the stratification effect engendered by the ejection of “digital ink” results in noticeable linear marks or striations that alter the texture and morphology of the printed part [5].

MJT, as reported in the ISO/ASTM 52900:2021, is an AM category in which droplets of 3DP material are selectively deposited [6]. This technology is a full-color 3DP process, which directly deposes resins in CMYK-W (cyan, magenta, yellow, black, and white) when required. Furthermore, MJT technology reproduces color gradients and variations unavailable with other 3DP technologies. Therefore, MJT plays a vital role in full-appearance reproduction.

Both conventional and advanced manufacturing technologies recognize the importance of surface quality in final products, mainly for critical and small products. Thus, it is essential to assess the surface finish of as-printed polymers and offer guidance on AM process windows and limitations to increase their applicability. To enhance the appearance of materials, 3DP systems must capture the optical properties of materials, communicate the attributes related to appearance, scan, model, and control 3D printing systems. Surface issues hinder the development of the workflows for the full appearance of materials during the design and manufacturing phases [7].

Appearance assessment is qualitative, subjective, and controversial [8]. An instrumental appearance measurement is an indirect technique for evaluating the quality and processing performance of a manufactured product based on its surface. Quality control has evolved into an industry concept through controlling color, gloss, haze, scattering, transparency, and texture, describing the “total appearance” [8]. Among these appearance attributes, the level of transparency, i.e., translucency,

* Corresponding author.
E-mail address: ali.p.golhin@ntnu.no (A. Payami Golhin).

https://doi.org/10.1016/j.optlastec.2023.109992
Received 28 April 2023; Received in revised form 6 August 2023; Accepted 22 August 2023
Available online 25 August 2023

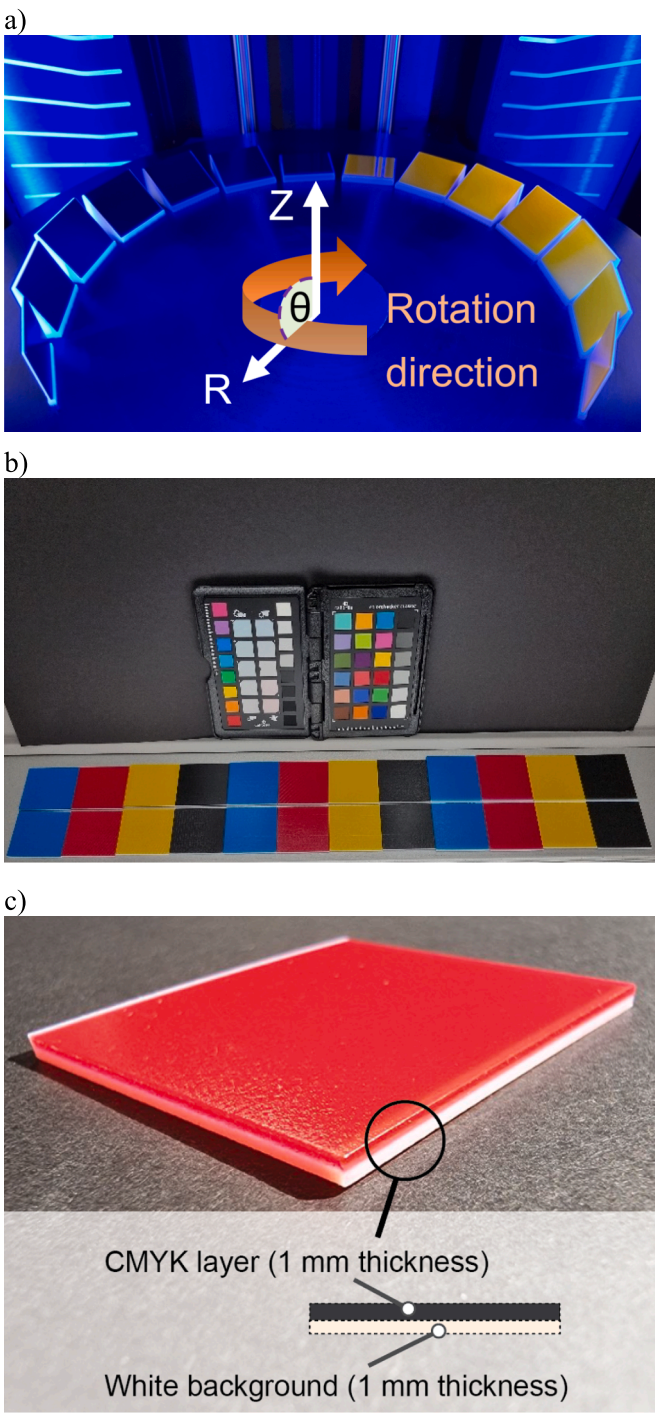

Fig. 1. A) as-printed YK specimens as seen on the rotary build platform, b) CMYK specimens observed under d50 daylight standard illumination, and c) layer configurations.

plays a defining role in the optical properties of MJT parts, affecting other characteristics as it describes how light travels through a medium.

Even though the surface finish of MJT parts was assumed to be consistent and detailed with minimal layering [9], the conditions of drop-on-demand high-speed manufacturing of translucent materials significantly affect their appearance. In the rotary-based MJT technique using PolyJet® machines, the objects are created by jetting materials onto a rotary tray as the build plate. Since each droplet of material contains its own mini pool of ink, the shape of the voxels and layers can be affected by printing parameters [10]. Therefore, MJT products can be designed in various approaches, bringing flexibility and manufacturing challenges. In aesthetic applications, such as jewelry [11] and medical models [12], the shape and combination of voxels are essential factors. For instance, MJT offers new possibilities for medical models due to its potential for manufacturing more realistic and patient-specific models. In contrast to fused filament fabrication (FFF) with a roughness average (R_a) of 1 μm to 30 μm [13,14], MJT offers more control on the surface roughness (R_a less than 10 μm) [14]. It also provides a superior high-detailed appearance of as-printed objects. However, the dimensional accuracy and appearance of a 3D object must be accurately reproduced using multiple printer parameters to achieve high-fidelity reproductions [15].

The material jetting process faces various technical challenges, including printability issues, material considerations, process optimization, and post-processing challenges [14]. These issues can significantly impact the quality and functionality of printed objects. Printability issues, such as nozzle clogging or misalignment, can lead to distorted or incomplete prints, while material considerations involve selecting compatible materials that produce desired properties in the final product. Issues with material properties, such as viscosity and drying behavior, or compatibility problems between multiple materials result in defects in printed parts. While post-processing is ultimately considered to lead to the desired properties, it poses many limitations, such as cost, availability, removing support structures, quality assurance of the surface finish, and curing or drying printed parts [14]. The optimization of processes is crucial in reducing post-processing demands. It improves efficiency and accuracy by fine-tuning parameters like layer thickness and printing speed, balancing printing speed/quality [16], finding optimal printing parameters [17], overcoming limitations in material properties, waste management, and optimizing material usage.

Limited research [18,19] has been conducted on the influence of build orientation (BO), also known as wedge/slope angle, on the surface quality of additively manufactured parts. In MJT, BO can affect the mechanical performance of manufactured parts. Abayazid et al. [20] showed prints along the Z-direction had the greatest influence of orientation on loading response, especially at larger strains and slower strain rates. Khoshkhoo et al. [21] studied the influence of BO on dimensional accuracy in MJT. They indicated that BO significantly influences thin sections rather than the dimensional precision of thicker components.

The bidirectional reflectance distribution function (BRDF) was initially introduced as a fundamental radiometric concept. BRDF captures all the details of how light interacts with surfaces [22,23]. The alteration of the appearance of MJT parts due to printing parameters has been studied in limited research [15,24,25]. However, it is yet to be shown whether these various attributes can be studied simultaneously in rotational MJT. Besides, no studies have addressed the significance of BO for 3DP tilted surfaces on a rotary disc.

This study examines the influence of BO on the various appearance attributes of MJT surfaces. For this purpose, the color, gloss, haze, scattering, transparency, and texture of the PolyJet parts were characterized as part of the quality improvement approach of AM surfaces. Based on the Kendall rank correlation coefficient and principal component analysis (PCA), the results were ranked, and possible correlations were discussed.

2. Materials and methods

2.1. Manufacturing process

The polymeric tilted surfaces were manufactured using a Stratasys J55 PolyJet 3D printer. The GrabCAD Print software was employed to import 3D models and subsequently printed in the standard tray material, which allows for a mixture of over 500,000 unique color combinations. Photo-resins VeroCyan, VeroBlackPlus, VeroYellow, VeroMagenta, and VeroPureWhite were used as feedstocks, hereafter

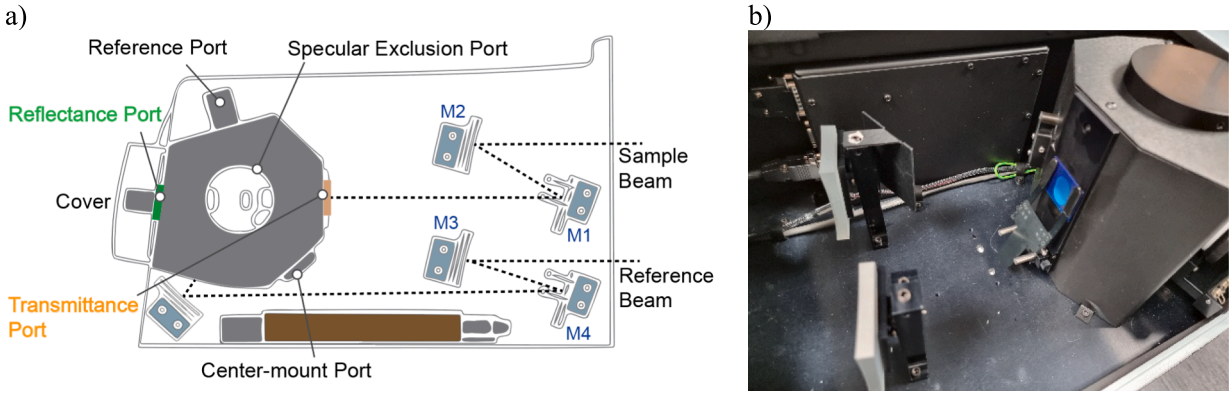

Fig. 2. A) schematic of the UV/VIS/NIR spectrometer in top view, and b) the measurement geometry of the sample (cyan color) located on the transmittance port.

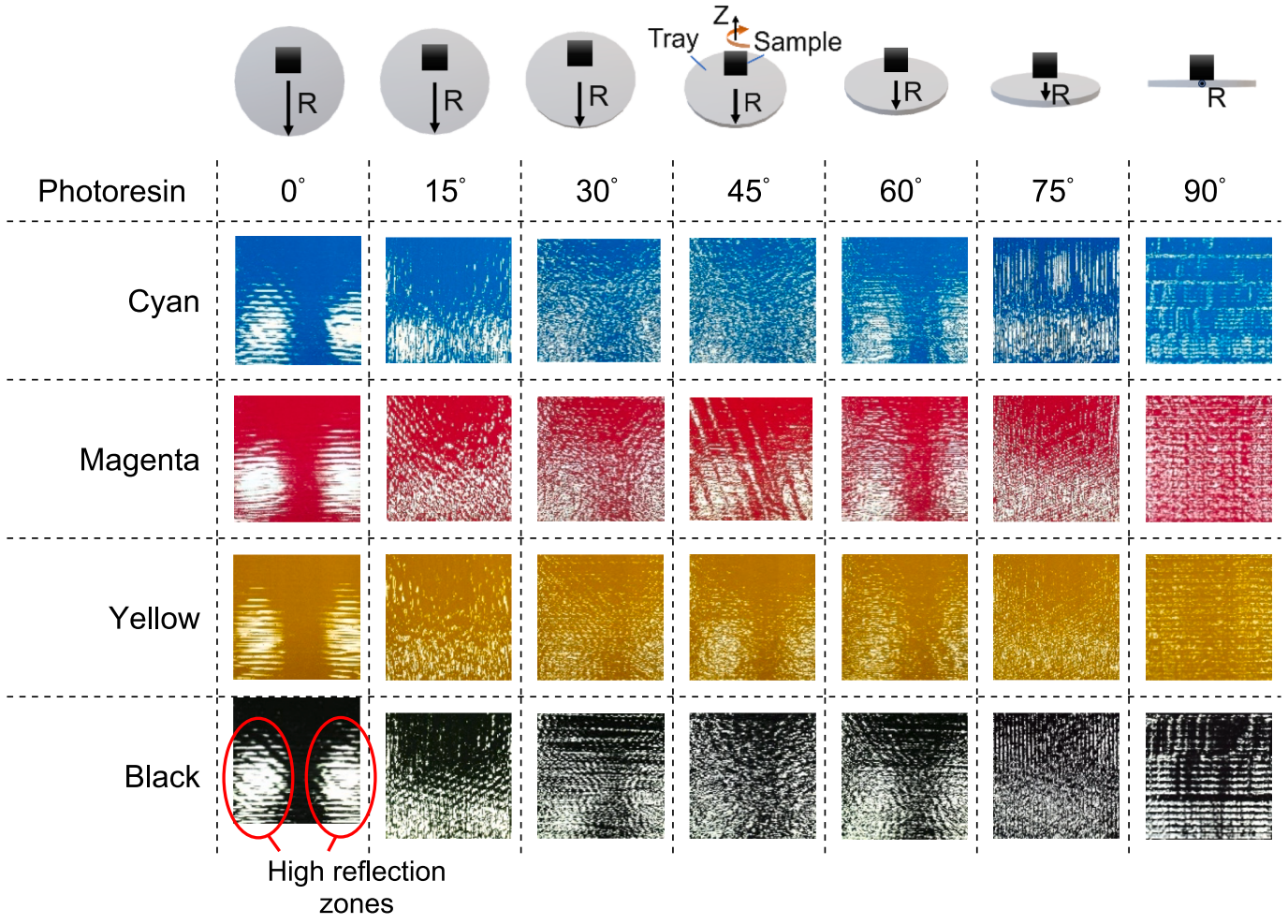

Fig. 3. The influence of build orientation on surface texture variability in material jetting products. The schematic above the figure displays the corresponding normal view of the sample for each BO corresponding to the rotary tray.

referred to as their corresponding colors of "C: cyan", "M: magenta", "Y: yellow", "K: black", and "W: white". In the Vero materials, acrylic oligomers are mixed with proprietary components to provide low-viscosity materials. Photo-resins from Vero share similar mechanical, thermal, and electrical properties [26]. CMYK photoresin (digital material) specimen was printed with seven different build orientations ranging from 0° (reference) to 90° at intervals of 15° (Fig. 1). According to the best practices of Stratasys for PolyJet and Pantone's guidelines for color matching [27], bilayer structures were constructed using 1 mm thick plates of each CMYK color on a 1 mm thick white background to achieve optimal color reproduction (Fig. 1c). Each sample was 35.5 ± 0.5 mm wide, 40.0 ± 0.5 mm long, and fabricated on the middle swath of a rotary disc as the build platform with a glossy-on-glossy finish. A waterjet system was used to remove the support waxes. To ensure the reproducibility of the results, the appearance characteristics of each specimen were measured five times using two sets of specimens.

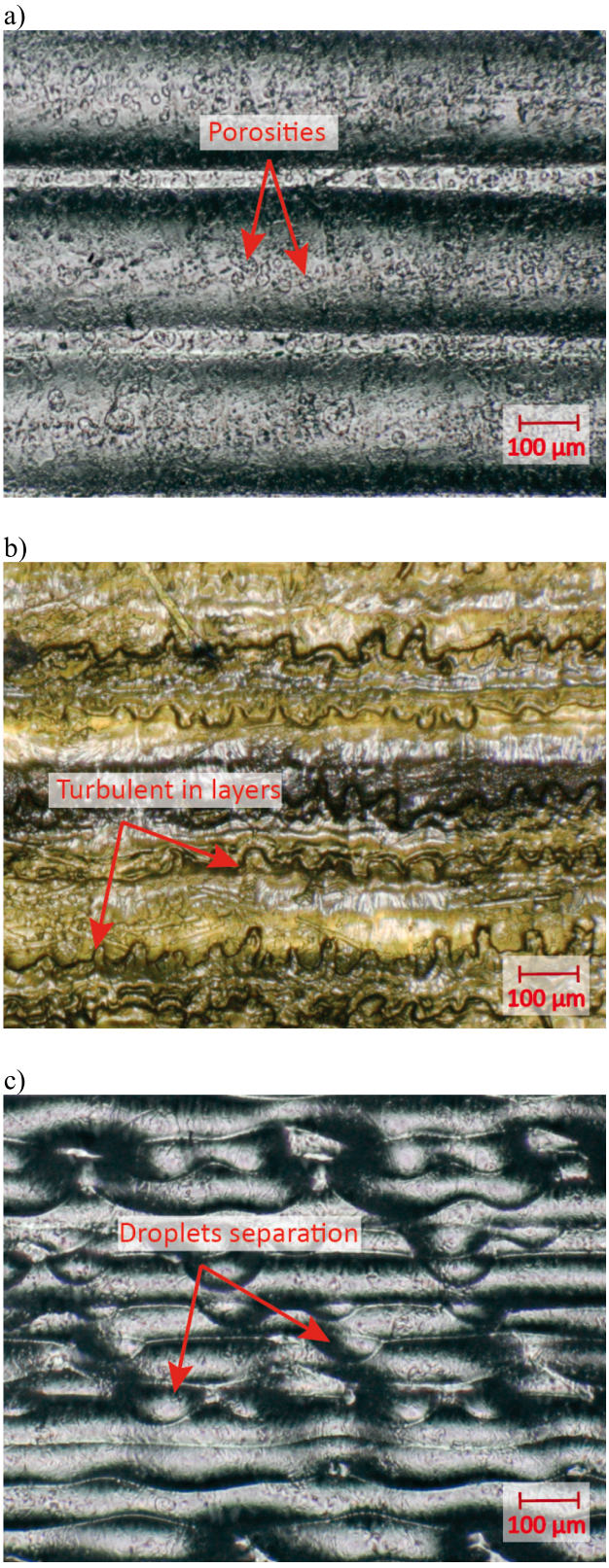

Fig. 4. Focal microscopic images of a) bilayer - BO 0°, b) monolayer of the colored plate - BO 0°, and c) bilayer - BO 15°.

2.2. Appearance measurement

A Keyence VH-ZST microscope was used for optical microscopy (20X to 2000X). The RA-532H surface reflectance analyzer was used to analyze gloss according to ASTM D523, haze, and scattering. The scattering results were discussed in terms of the C20 and C60 Canon scattering indices for illumination angles of 20° according to ASTM D5767 and 60° as per JIS K7374, respectively. In computer graphics, the C20 index measures the distinctness of the image (DOI), while the C60 index measures the clarity of the image (IC).

The spectroscopy was conducted using a spectrometer (PerkinElmer Lambda 1050 +) equipped with the 3-detector module in an integrating sphere configuration (150 mm). Spectra of reflectance, transmission, and absorbance were measured from photopolymer plates aligned in the detector window. The wavelength length was limited to 380 to 780 nm and sampling intervals of 5 nm. The largest area possible in the middle of the specimens was exposed to a light beam to minimize the effects of layer-by-layer inhomogeneity and edge effects caused by light scattering. The measurement area was therefore limited to the size of the reflectance (24 mm in diameter) and the transmittance (25 mm × 16 mm) ports (Fig. 2). Transmittance data were recorded from the front (F) and back (B) of the specimens. The measurement error was reduced by avoiding sites with support materials, unusual colors, stains, and external particles.

To calculate tristimulus values, CIEXYZ, a color-matching function derived from ASTM E308-01 [28], was applied using CIE 2° and the D50 standard daylight illuminant. CIEL*a*b* coordinates were further determined using CIE1976. The CIEDE2000 color differences for each BO compared to the 0° orientation were calculated using the computational color science toolbox in MATLAB R2022a [29] as follows

$$CIEDE2000 = \sqrt{\left(\frac{\Delta L^*}{k_L S_L}\right)^2 + \left(\frac{\Delta C^*}{k_c S_C}\right)^2 + \left(\frac{\Delta h^*}{k_h S_h}\right)^2 + R_T f(\Delta C^* \Delta h^*)} \quad (1)$$

where color attributes vary due to the color change expressed by ΔL^* (lightness), ΔC^* (chroma) and Δh^*(hue), R_T corresponds to the hue rotation, S_L, S_C, and S_h communicate CIEL*C*h* lightness compensation, and k_L, k_C, and k_h constants were defined as unity.

A Vizoo xTex scanner was used to collect texture data, including displacement, material, alpha, base, surface roughness, and surface normals. With the Blender 2.79 render engine, the 2D surface texture maps were further applied onto 3D spherical models.

2.3. Statistical analysis

The mean color difference from the mean (MCDM) and the corresponding root-mean-square error (RMSE) variables were used to discuss the color difference according to CIEDE2000 using the following equations

$$MCDM = \frac{1}{N}\sum_{i=1}^{N} \Delta E(C_i, C_m) \quad (2)$$

$$RMSE = \sqrt{\frac{1}{N}\sum_{i=1}^{N} (r_{r,i} - r_{t,i})^2} \quad (3)$$

where r_t and r_r are the tests and references spectral results for N samples. C_i and C_m indicate the color coordinate of the i^{th} measurements and the reflectance average, respectively.

To assess spectral deviations among transmittance and reflectance results in different BOs compared to horizontal samples (0°), Kendall's tau (τ) rank correlation coefficients were employed. Statistical significance is well-defined when the p-value is less than 0.05 [30]. It is an appropriate measure of the strength of association between continuous-ordinal variables or two ordinal variables. Kendall's τ helps identify monotonic relationships due to its resistance to outlier effects [31].

Principal component analysis (PCA) was applied to examine the spectral data and response variables. For matrices that contain dependent and independent variables, PCA extends linear regression to a

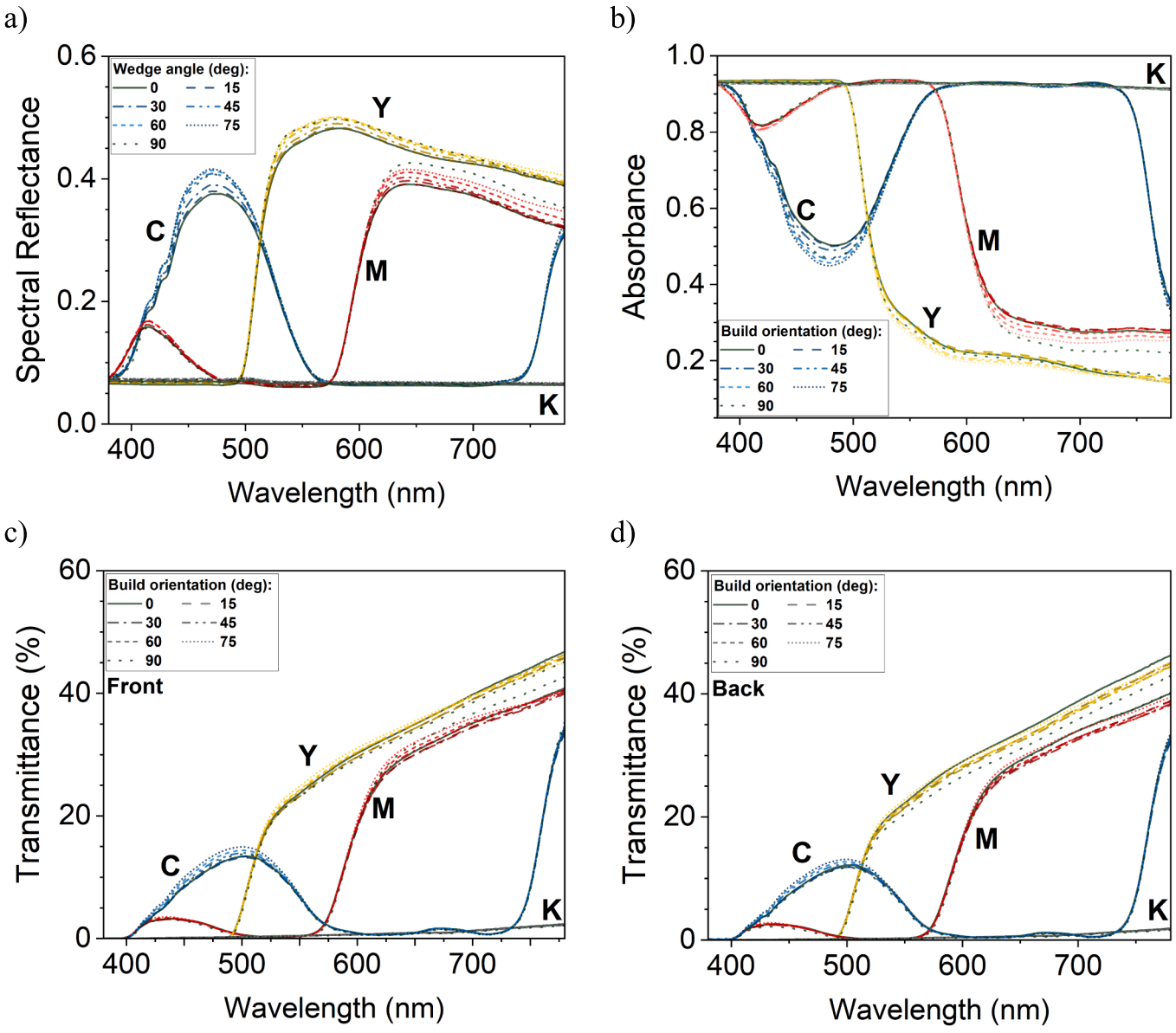

Fig. 5. A) spectral reflectance, b) absorbance, and transmittance from c) front and d) back of MJT specimens with tilted surfaces.

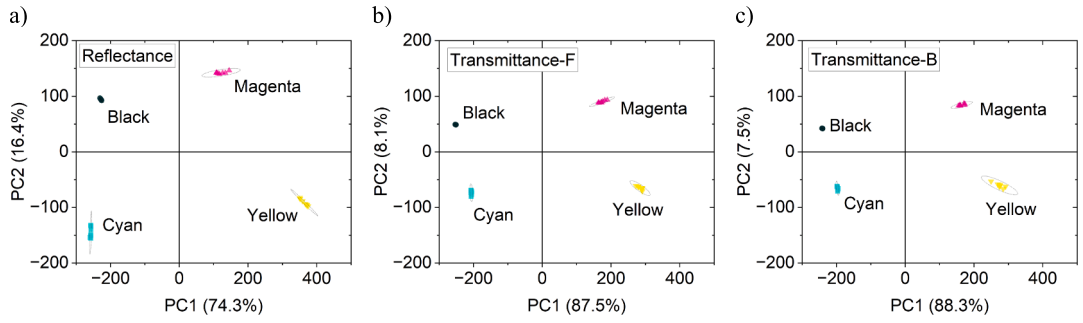

Fig. 6. PCA results for a) spectral reflectance (CPV: 90.71%), and transmittance from b) front (CPV: 95.59%) and c) back (CPV: 95.78%) of MJT specimens. The ellipses represent 95% confidence of PCA score data (BOs).

multivariate setting [30]. Considering the first batch (build orientation) as an independent variable, and the second batch (spectral data) as a dependent variable, it is possible to view the two sets of variables as asymmetrical. This study used two types of PCA to evaluate the data: ordinary PCA to assess the BO effect and spectroscopy PCA to consider the material impact on the spectral variables. The raw sensor data was converted using linear transformation into principal components (PCs) space. R statistical software 4.2.1 and Origin 2022 (OriginLab) were

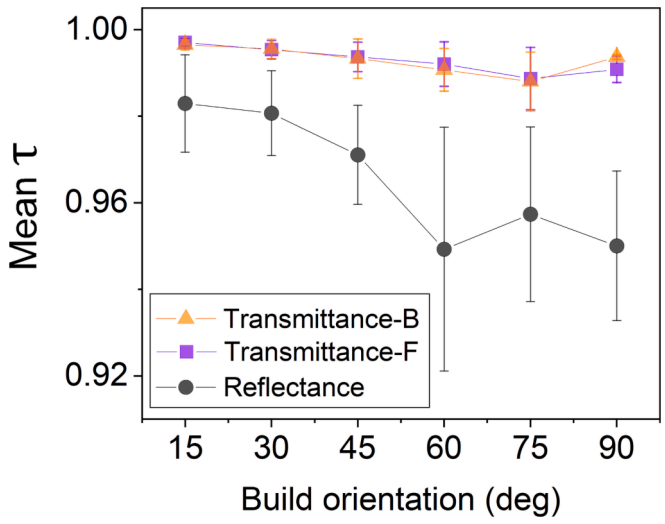

Fig. 7. Kendall's τ rank correlation coefficient in the spectrophotometry measurements of tilted surfaces according to the horizontal reference surface (Error bars: RMSE).

used to analyze the data.

3. Results and discussions

3.1. Optical microscopy

In Fig. 3, a micro digital camera was used to illustrate the variation in the surface texture of MJT objects manufactured at various BO ([0°-90°], 15° step) as seen in the manufacturing workspace. The direction in which the printing was performed significantly affected the surface texture, resulting in a variation in the distribution of high-exposure reflections on the surface. A distinct difference in surface texture and structured layers can be seen for 0° compared to other angles. BO affected the gloss variation and waviness in the printed layers. In particular, smooth, high-gloss, and layered structures produced by horizontal 3D printing (BO 0°) differ from rough and structurally distinct surfaces generated in a vertical direction (BO 90°), which were less affected by the rotation of the build platform (rotary tray) in the vertical orientation. As illustrated for the K-0° sample in Fig. 3, the repeated white zone pattern exhibiting higher light reflectance is more significant for BO 0° compared to other BOs, particularly 30° and 60°. It can be explained by the rotation pattern of the tray and jetting operation by the printhead during layer formation from the inner to the outer area of the tray. Further elaboration on the appearance and reflection of light is provided in the spectral reflectance and gloss results.

Fig. 4 provides a closer look at the full focal images of MJT surfaces without being affected by specular reflections. The surface printed at the horizontal reference orientation (0°) can be described by parallel and horizontal microscopic layers with porous surfaces due to incubated gas release on the surface (Fig. 4a). Furthermore, focal images in Fig. 4b revealed subsurface turbulence in layers in the 1 mm thick translucent-colored layer (see Fig. 1b). Light transmission affected by microscopic inhomogeneities within the subsurface layers (3D-printed patterns) was discussed within the transmittance results. Fig. 4c illustrates how tilting the surface at 15° significantly altered the order of microscopic layers due to the separation of microscopic droplets. Thus, with an increase in BO, the number of parallel horizontal patterns observed also increased, indicating more surface features due to the printing along both the R and Z directions (see Fig. 3). Several factors can explain the reason behind the appearance of the presence of cured ink droplets and more surface layers at BO 15°. The rotation speed of the disc-shaped build platform and the corresponding centrifugal force, viscosity, and resin mass, may unveil the reason behind the shapes of surface features. Accordingly, the jetting pattern at different BO, printing speeds, and the UV curing process were influenced. Comparable to alternative methods of material joining, such as welding [32], the configuration and morphology of ink pools indicate the underlying dynamics of fluid flow, cooling mechanisms, and the transition from liquid to solid state.

3.2. Spectral analysis

Fig. 5 illustrates spectral data, including reflectance, absorbance, and transmittance. According to the spectrophotometry results, there was a spectral shift for different BOs in CMY resins. However, the black color did not significantly change the spectral characteristics at various BOs. In Fig. 5a, reflectance values increased with increasing BO, indicating higher lightness (albedo) at higher wedge angles. In the case of absorbance (Fig. 5b) and transmittance (Fig. 5c and d), this shifting behavior was dependent on the digital material. For cyan, higher transmittance and lower absorbance were observed, while yellow and magenta resins showed lower levels of transmittance and absorbance. The transmittance spectra resulting from spectrometry in the broader wavelength range, including near-infrared (NIR), are presented in the supplementary data in Appendix A.

The PCA results in Fig. 6 suggest two principal components of PC1 and PC2 with a cumulative percentage variance (CPV) of greater than 90.71%, adequately explaining the observed behavior in the spectral

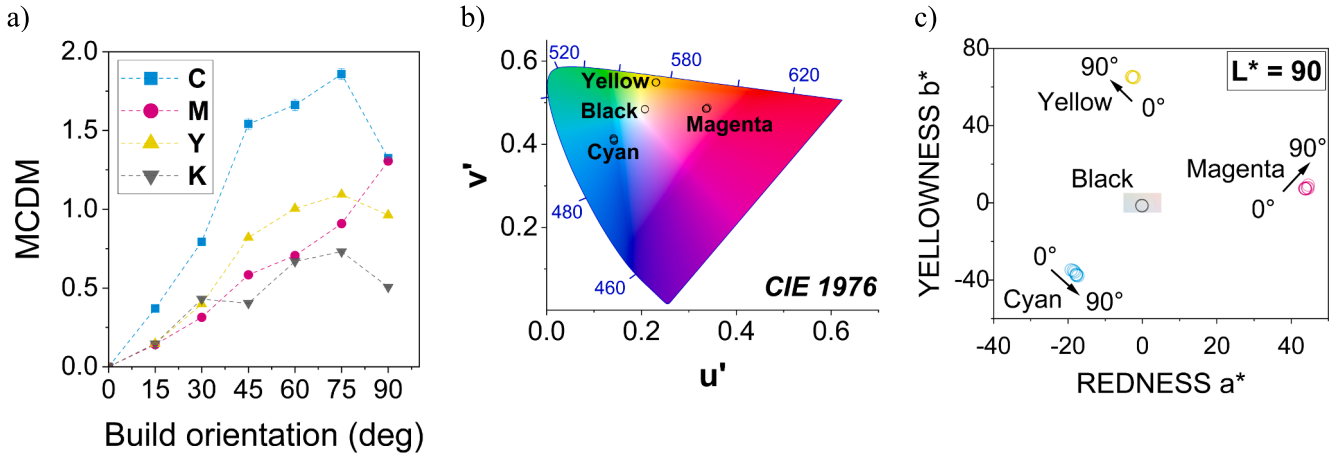

Fig. 8. A) MCDM of color difference, b) the mean hue u', v' stimuli according to cie1976 chromaticity diagram, and c) color change in CIEL*a*b* color space. Vectors represent color change as a result of using different BO.

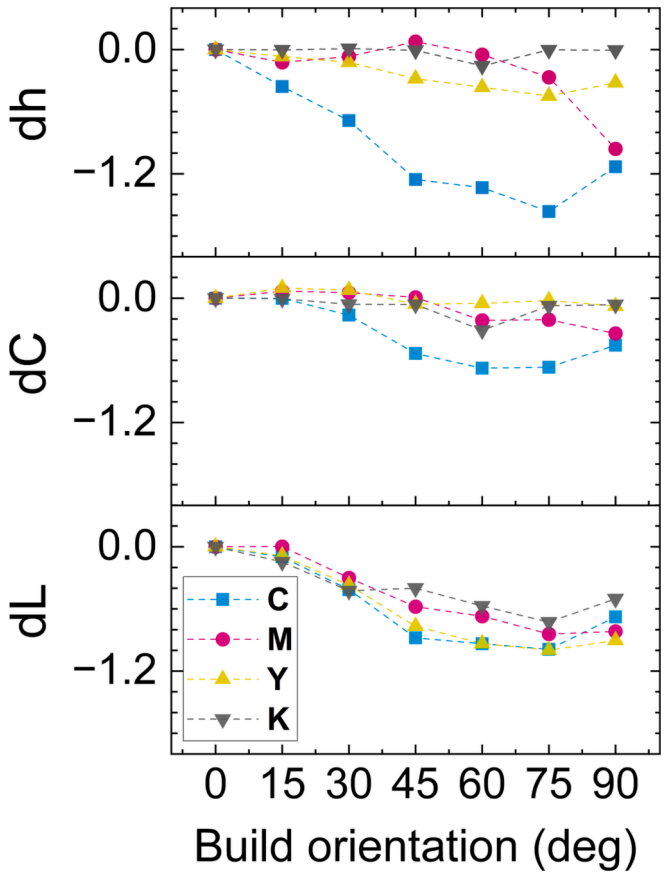

Fig. 9. Variations in color attributes due to changing the build orientation.

data. The CMYK materials were used as the observation group, and the spectral results addressed the studied variables. The results revealed the same pattern in the PCA results for both reflectance and transmittance. The spectral shifts in the spectrophotometry results can be explained by considering their PCA score distribution. According to the results, PC1 affected magenta and yellow positively while negatively impacting black and cyan. By contrast, PC2 had a negative impact on cyan and yellow, and it had a positive influence on magenta and black.

Furthermore, the score distribution, i.e., the 95% confidence ellipses for the studied BO angles, indicated a higher impact on yellow from both PC1 and PC2 than particularly on black. Furthermore, magenta scores were affected more by PC1, while cyan scores were altered more according to the PC2 axis, indicating opposite responses due to manufacturing different wedge angles. The similar behavior of front and back transmittance measurements showed that the reflectance and absorbance had a negligible effect on light transmission through the CMYK layers joint with a white background.

Fig. 7 demonstrates how different BOs affect the optical properties of the manufactured surface in the spectrophotometry measurement compared to horizontal 3D-printed surfaces, regardless of the applied material. While BO 75° resulted in more deviation in transmittance measurements ($\tau_F = 0.989$ and $\tau_B = 0.988$), BO 60° ($\tau = 0.949$) and then 90° (vertical orientation, $\tau = 0.950$) led to more significant spectral shifts in reflectance measurements. Kendall's τ rank correlation results revealed a more substantial influence of variation in the texture and manufactured layers due to different BOs on the reflectance results compared to transmittance. The RMSE was also higher for the reflectance spectra, where it is maximized at a critical BO 60° (RMSE = 0.028) for the reflectance spectra and 75° (RMSE = 0.007) for the transmittance spectra. Strong correlations with τ greater than 0.949 and p-value less than 0.050 were observed for all studied materials. Appendix B provides supplementary data for statistical analysis of PCA and τ rank correlation results for each pair of build orientation.

The color measurement results are displayed in Fig. 8 to evaluate the effects of spectral reflectance on the visual appearance. As shown in Fig. 8a, MCDM generally increased and peaked at a BO angle of 75° before decreasing for cyan, yellow, and black materials. For magenta resins, however, the increase in color difference due to a rise in BO angle was constant and even sharper for 90°. As shown in Fig. 8b and c, a weak alteration in color has been observed due to BO, which was more pronounced for cyan, magenta, and then yellow when compared to black resins. For all studied materials, the MCDM was less than 2, and the RMSE was negligible, indicating high color fidelity and barely noticeable color differences due to tilting the surface.

Fig. 9 shows that all color attributes (LCh) were shifted to negative values, where similar trends were observed for all materials based on their MCDM. Magenta showed high dL at 90°, whereas cyan, yellow, and black had a robust negative shift in lightness at 75°. Hue and chroma also demonstrated the same trend. The variations in lightness were, however, generally more substantial than hue and chroma. This

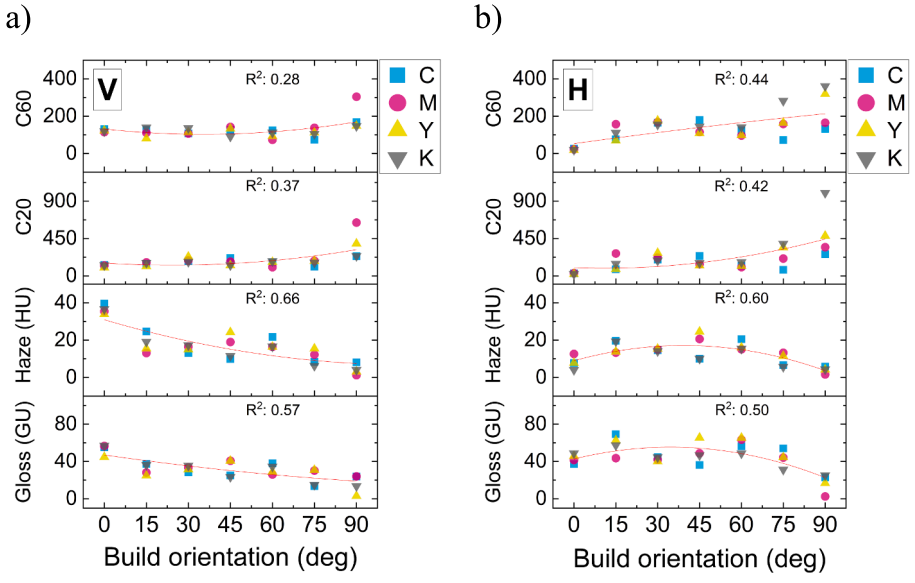

Fig. 10. Fitting results of the mean for gloss nuances in a) vertical and b) horizontal measurement directions according to the directions of the layers.

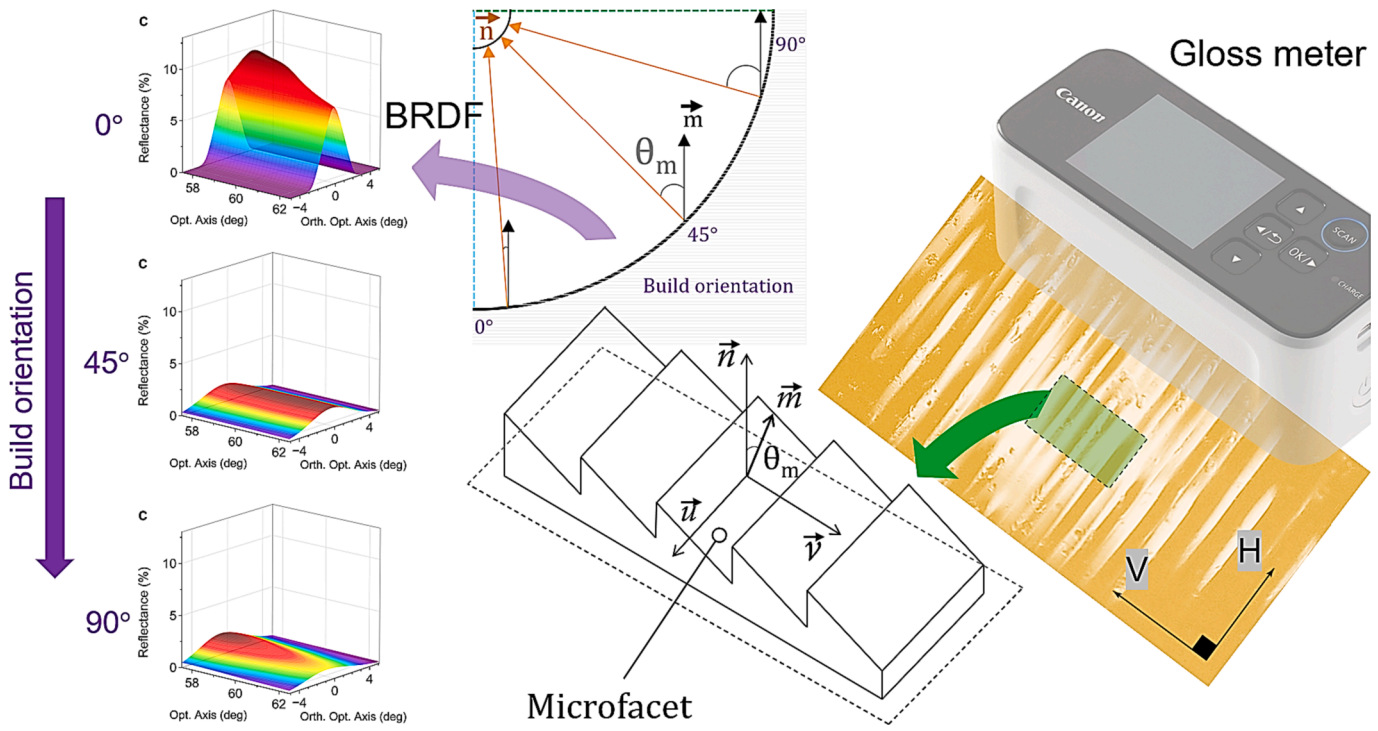

Fig. 11. Gloss measurement of textured AM surfaces. BRDF graphs represent light distribution around vertical measurements around the angle of 60° for BO 0°, 45° and 90° for the cyan specimen.

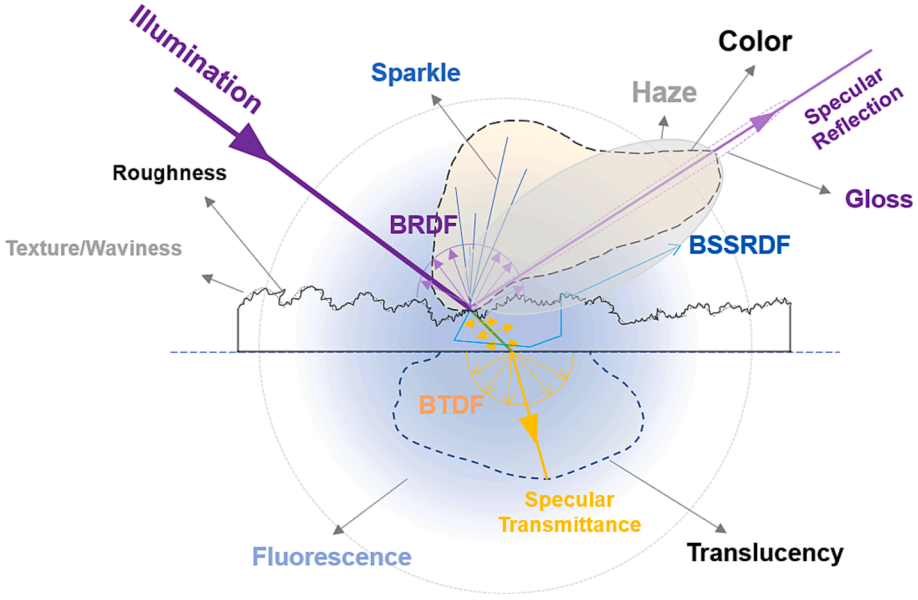

Fig. 12. Light-matter interactions and optical properties of textured surfaces. BSSRDF: Bidirectional scattering-surface reflectance distribution function.

indicates lightness change has a significant role in reflectance due to the alteration in surface texture caused by build orientation.

3.3. Gloss measurement

Fig. 10 compares several aspects of gloss appearance, including specular gloss, haze, and scattering indices of C20 and C60 derived from BRDF. As can be seen from the fitting lines in the vertical (V) and horizontal (H) directions according to layer-by-layer structures, the measurement direction affected the gloss measurements. The specular gloss and haze decreased more linearly with increasing BO angles in the V direction. Conversely, the H direction resulted in nonlinear behavior, with gloss and haze maximized at 45° to 60° degrees of BO. The BO 90° displayed a distinct low-gloss and low-haze characteristic, as well as high scattering, in both measurement directions. Nevertheless, results indicated that an increase in BO led to an increase in the C20 and C60 indices representing scattering. A high level of R^2 suggested a stronger correlation between BO and haze and specular gloss as opposed to sublayer scattering, which was in agreement with the spectral results observed for reflectance compared to transmittance.

According to the V measurement direction (Fig. 10a), gloss and its surrounding haze display higher specular reflections for lower BO

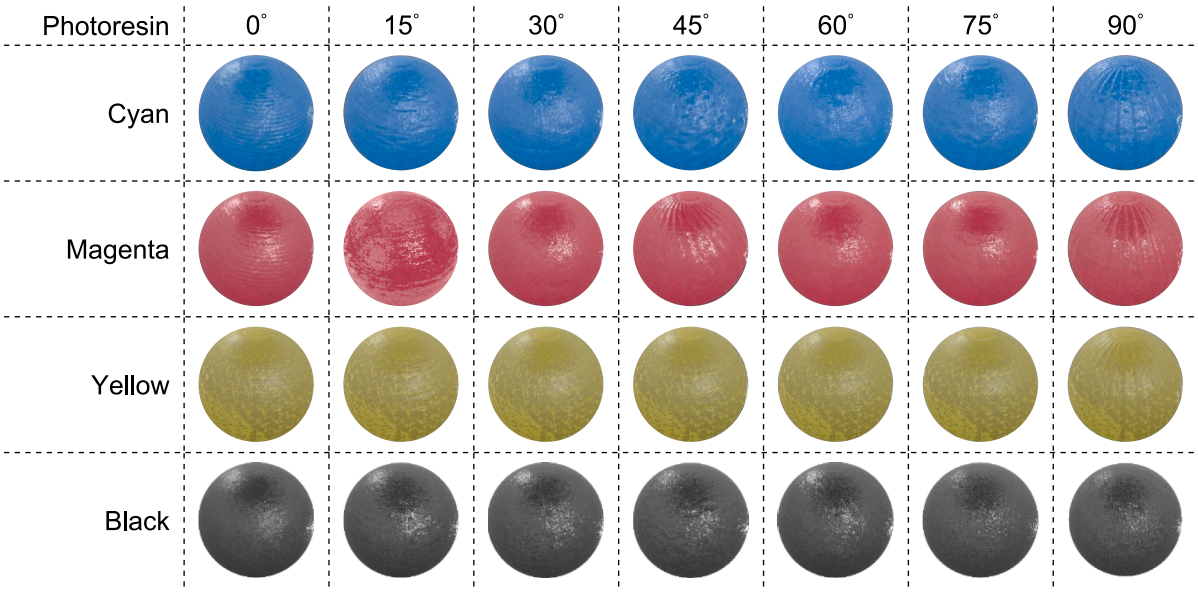

Fig. 13. 3D-rendered sphere models from optical texture mapping of 3D-printed CMYK digital materials with different build orientations.

angles. Reflected haze is characterized by a milky or cloudy appearance due to light scattering [33]. Haze is considered an appearance attribute that refers to lower surface quality due to defects, including surface texture or porous surface (see Fig. 4), as part of the assessment of surface quality.

Fig. 11 illustrates the importance of the direction and size of microsurfaces in textured surfaces influenced by building orientation. Bidirectional reflectance distribution function (BRDF) graphs decreased in size at higher BO, indicating a decline in reflectance, resulting in lower gloss and haze. The supplementary data in Appendix C contains more BRDF graphs for gloss measurements.

Higher gloss and haze for lower BOs can be attributed to larger microsurfaces and lower θ_m. This resulted in stronger microsurface normals that were closer to the surface normals determined by $\cos\theta_m$. As a result, gloss and haze are significantly higher at BO 0° where microfacet's normal ($\vec{m}$) is acting similarly to the surface normal ($\vec{n}$), which was normal to the surface reflectance analyzer. However, in the horizontal direction, a slight curvature in the layers, as seen in our previous study [15], and subsurface turbulence in layers played a more important role compared to microsurface variations due to BO. It resulted in a more nonlinear behavior in gloss nuances for horizontal glass measurement (Fig. 10b).

Microfacets' role in translucent textured surfaces can be explained by Fresnel's equation [34], using bidirectional scattering distribution functions (BSDF)

$$f_{r,m}\left(x_m, \vec{\omega}_i, \vec{\omega}_o\right) = F\left(\vec{m}, \vec{\omega}_i, \frac{n_t}{n_i}\right) \frac{\delta\left(\vec{\omega}_o - \vec{\omega}_s\right)}{\cos\theta_i} \tag{4}$$

where the $f_{r,m}$ term denotes the reflectance from a smooth microsurface in a semi-transparent part for a specific surface point (x_m), considering the unit light vectors for illumination $(\vec{\omega}_i)$, scattering $(\vec{\omega}_s)$, and observation $(\vec{\omega}_o)$. The expansion of Maxwell's equations using the Fourier transform is referred to as F for the unit of the surface, where n_t and n_i represent the transmission and illumination normals. The Dirac δ function applies to observation and scattering unit vectors of lights. The illumination angle relative to the surface normal ($\vec{n}$) is shown by θ_i.

BSDF comprises both reflectance and transmittance terms for the same macroscopic surface point from which light is incident and emerges [35]. It can be regarded as the sum of BRDF and BTDF (bidirectional transmittance distribution function), as shown in Fig. 12.

3.4. Surface texture mapping

Fig. 13 illustrates the use of optical surface maps to create textured spheres. In contrast to the black and yellow resins, cyan and magenta clearly displayed the layer's orientation fabricated in the manufacturing process. The parallel layers were particularly evident in BO 0°, 45°, and 90°. The low absorption of yellow materials made optical texture mapping more challenging to render than other digital materials.

4. Conclusions

This study discussed how build orientation affects the optical properties of 3D-printed objects in material jetting, which is a necessary step toward reproducing full-color appearances. CMYK colors were applied using the primary digital materials in PolyJet 3D printers. Color, gloss, haze, scattering, and transparency were characterized, leading to the following conclusions.

A microscopical examination revealed that various BOs resulted in different textures and surface characteristics, including layer configurations, gas porosities, droplet separation, and subsurface turbulence in layers. Microscopic inhomogeneities affected the optical properties of translucent MJT materials.

As shown by spectrophotometric analysis, tilted CMY surfaces exhibited more variation in reflectance, transmittance, and absorbance compared to black photoresin. Based on PCA score distribution, although each photoresin responded differently to the principal components, the same pattern of variation of the materials studied was observed for both reflectance and transmittance. The Kendall rank correlation coefficient for transmittance measurements indicated that BO 75° resulted in a more significant deviation. In terms of reflectance, BOs 60° and then 90° resulted in the largest spectral shifts. The texture and manufactured layer variation caused by various BOs impacted the reflectance more than the transmittance results.

A substantial effect of measurement direction on gloss, haze, and scattering results was observed compared to color appearance, indicating the importance of microsurface normal direction on the gloss measurements. Gloss and haze in vertical measurement directions decreased significantly when the surfaces were tilted from 0° to 90°. The subsurface scattering results, however, increased with the increase in BO, regardless of the measurement direction.

Overall, the results confirmed the significant effect of BO on the surface texture and layer orientation, leading to a variation in surface

quality due to its impact on appearance attributes. The results also suggest that the measurement direction of the gloss meter position of the target significantly affects the gloss measurements in additive manufacturing. Furthermore, gloss and scattering were more critical than the color appearance in the optical assessment.

For future studies, it is expected that full-color 3D printing will acquire significant attention in terms of process optimization. Computational fluid dynamics and numerical techniques for the simulation of manufacturing processes can enhance the knowledge of induced anisotropic arrangements and their impact on manufacturing and product properties. Furthermore, it is necessary to conduct further research on the materials application procedure and the actual stress, heat, and aging that will affect the texture and appearance of objects in material jetting.

CRediT authorship contribution statement

Ali Payami Golhin: Conceptualization, Methodology, Investigation, Data curation, Formal analysis, Visualization, Writing – original draft, Writing – review & editing. **Are Strandlie:** Writing – review & editing, Supervision, Project administration, Funding acquisition.

Declaration of Competing Interest

The authors declare the following financial interests/personal relationships which may be considered as potential competing interests: [Ali Payami Golhin reports financial support, and article publishing charges were provided by Horizon 2020 (EU) ApPEARS-ITN project [grant No. 814158].

Data availability

Data are available at https://doi.org/10.5281/zenodo.7579455

Acknowledgments

This work is funded by the European Union's H2020 research and innovation program under the Marie Skłodowska-Curie grant agreement No. 814158 "ApPEARS - Appearance Printing - European Advanced Research School". The authors appreciate the support provided by Dr. Andreas Kraushaar (Fogra, Germany) and Donatela Saric (NTNU & Fogra) for the gloss measurement. The authors would like to thank Dr. Aditya Suneel Sole (NTNU, Norway) for his support and contributions to this work.

Appendix A. Supplementary material

Supplementary data to this article can be found online at https://doi.org/10.1016/j.optlastec.2023.109992.

References

[1] H.E. Quinlan, T. Hasan, J. Jaddou, A.J. Hart, Industrial and consumer uses of additive manufacturing: A discussion of capabilities, trajectories, and challenges, J. Ind. Ecol. 21 (2017) S15–S20, https://doi.org/10.1111/jiec.12609.
[2] S. Rouf, A. Raina, M. Irfan Ul Haq, N. Naveed, S. Jeganmohan, A. Farzana Kichloo, 3D printed parts and mechanical properties: Influencing parameters, sustainability aspects, global market scenario, challenges and applications, Advanced Industrial and Engineering Polymer Research (2022), https://doi.org/10.1016/j.aiepr.2022.02.001.
[3] A. Payami Golhin, C. Srivastava, J.F. Tingstad, A.S. Sole, A. Strandlie, S. Grammatikos, Additive manufacturing of multilayered polymer composites: Durability assessment, in: Proceedings of the 20th European Conference on Composite Materials-Composites Meet Sustainability (Vol. 1-6), EPFL Lausanne, Composite Construction Laboratory Switzerland, Lausanne, Switzerland, 2022, pp. 298-305. doi:10.5075/epfl-298799_978-2-9701614-0-0.
[4] A. Payami Golhin, C. Srivastava, A. Strandlie, A. Suneel Sole, S. Grammatikos, Effects of accelerated aging on the appearance and mechanical performance of materials jetting products, Mater. Des. 228 (2023), 111863, https://doi.org/10.1016/j.matdes.2023.111863.
[5] A.P. Golhin, A. Strandlie, Appearance evaluation of digital materials in material jetting, Opt. Lasers Eng. 168 (2023), 107632, https://doi.org/10.1016/j.optlaseng.2023.107632.
[6] R. Magisetty, N.S. Cheekuramelli, Additive manufacturing technology empowered complex electromechanical energy conversion devices and transformers, Appl. Mater. Today 14 (2019) 35–50, https://doi.org/10.1016/j.apmt.2018.11.004.
[7] A. Payami Golhin, A. Strandlie, P. John Green, The influence of wedge angle, feedstock color, and infill density on the color difference of FDM objects, J. Imaging Sci. Technol. 65 (2021) 1–15, https://doi.org/10.2352/J.ImagingSci.Technol.2021.65.5.050408.
[8] M.R. Pointer, Measuring visual appearance-a framework of the future. Project 2.3 measurement of appearance, (2003).
[9] B. Msallem, N. Sharma, S. Cao, F.S. Halbeisen, H.F. Zeilhofer, F.M. Thieringer, Evaluation of the dimensional accuracy of 3D-printed anatomical mandibular models using FFF, SLA, SLS, MJ, and BJ printing technology, J. Clin. Med. 9 (2020), https://doi.org/10.3390/jcm9030817.
[10] Y. Feng, J. Liu, H. Li, X. Ma, P. Du, K. Li, Y. Liu, Deposition behavior optimization of on-demand tin droplet with gravity based on piezoelectric micro-jet, Int. J. Heat Mass Transf. 192 (2022), https://doi.org/10.1016/j.ijheatmasstransfer.2022.122902.
[11] M. Di Nicolantonio, E. Rossi, P. Stella, in: Generative Design for Printable Mass Customization Jewelry Products, Springer Verlag, 2020, pp. 143–152, https://doi.org/10.1007/978-3-030-20216-3_14.
[12] B. Dorweiler, P.E. Baqué, R. Chaban, A. Ghazy, O. Salem, Quality control in 3D printing: Accuracy analysis of 3D-printed models of patient-specific anatomy, Materials 14 (2021) 1–13, https://doi.org/10.3390/ma14041021.
[13] J.D. Kechagias, S.P. Zaoutsos, Optimising fused filament fabrication surface roughness for a dental implant, Mater. Manuf. Process. 38 (2023) 954–959, https://doi.org/10.1080/10426914.2023.2176870.
[14] A.P. Golhin, R. Tonello, J.R. Frisvad, S. Grammatikos, A. Strandlie, Surface roughness of as-printed polymers: a comprehensive review, Int. J. Adv. Manuf. Technol. 127 (2023) 987–1043, https://doi.org/10.1007/s00170-023-11566-z.
[15] A. Payami Golhin, A.S. Sole, A. Strandlie, Color appearance in rotational material jetting, Int. J. Adv. Manuf. Technol. 124 (2023) 1183–1198, https://doi.org/10.1007/s00170-022-10536-1.
[16] J. Kechagias, V. Iakovakis, E. Giorgo, P. Stavropoulos, A. Koutsomichalis, N.M. Vaxevanidis, Surface roughness optimization of prototypes produced by polyjet direct 3D printing technology, in: OPT-i 2014 - 1st International Conference on Engineering and Applied Sciences Optimization, Proceedings, 2014, pp. 2877-2888.
[17] K.-E. Aslani, A. Korlos, J.D. Kechagias, K. Salonitis, Impact of process parameters on dimensional accuracy of PolyJet 3D printed parts using grey Taguchi method, in: MATEC Web of Conferences, EDP Sciences 2020 01015, doi: 10.1051/matecconf/202031801015.
[18] J.A. Gonzalez, J. Mireles, S.W. Stafford, M.A. Perez, C.A. Terrazas, R.B. Wicker, Characterization of Inconel 625 fabricated using powder-bed-based additive manufacturing technologies, J. Mater. Process. Technol. 264 (2019) 200–210, https://doi.org/10.1016/j.jmatprotec.2018.08.031.
[19] N. Mohammadian, S. Turenne, V. Brailovski, Surface finish control of additively-manufactured Inconel 625 components using combined chemical-abrasive flow polishing, J. Mater. Process. Technol. 252 (2018) 728–738, https://doi.org/10.1016/j.jmatprotec.2017.10.020.
[20] F.F. Abayazid, M. Ghajari, Material characterisation of additively manufactured elastomers at different strain rates and build orientations, Addit. Manuf. 33 (2020), https://doi.org/10.1016/j.addma.2020.101160.
[21] A. Khoshkhoo, A.L. Carrano, D.M. Blersch, Effect of build orientation and part thickness on dimensional distortion in material jetting processes, Rapid Prototyping J. 24 (2018) 1563–1571, https://doi.org/10.1108/RPJ-10-2017-0210.
[22] H. Shi, Y. Liu, C. He, C. Wang, Y. Li, Y. Zhang, Analysis of infrared polarization properties of targets with rough surfaces, Opt. Laser Technol. 151 (2022), https://doi.org/10.1016/j.optlastec.2022.108069.
[23] Y. Han, H. Sun, H. Guo, Analysis of influential factors on a space target's laser radar cross-section, Opt. Laser Technol. 56 (2014) 151–157, https://doi.org/10.1016/j.optlastec.2013.08.007.
[24] L. Zheng, C. Li, S. Yang, Analysis of color gamut in color 3D printing, Lecture Notes in Electrical, Engineering 600 (2020) 148–155, https://doi.org/10.1007/978-981-15-1864-5_21.
[25] Y.L. Cheng, K.C. Huang, Preparation and characterization of color photocurable resins for full-color material jetting additive manufacturing, Polymers (Basel) 12 (2020) 650, https://doi.org/10.3390/polym12030650.
[26] V. Stratasys, Realistic, Multi-Color Prototypes in Less Time, Stratasys Datasheet, in, 2022, pp. 1–4.
[27] Stratasys, 3D Printing with Pantone Colors, in, Stratasys Ltd., 2021, pp. 1-6.
[28] Astm, Standard practice for computing the colors of objects by using the CIE system, in (2018) 1–45.
[29] S. Westland, C. Ripamonti, V. Cheung, Computational colour science using MATLAB, John Wiley & Sons, 2012.
[30] Y. Xia, Chapter Eleven - Correlation and association analyses in microbiome study integrating multiomics in health and disease, in: J. Sun (Ed.), Progress in Molecular Biology and Translational Science, Academic Press, 2020, pp. 309–491, https://doi.org/10.1016/bs.pmbts.2020.04.003.
[31] C.A. Gotway, Statistical Methods in Water Resources, Technometrics 36 (1994) 323–324, https://doi.org/10.1080/00401706.1994.10485818.
[32] S. Baharnezhad, A. Golhin, In-situ measurement and finite element simulation of thermo-mechanical properties of AA 6063 aluminum alloy for MIG weldment,

Mater. Phys. Mech. 32 (2017) 222–236, https://doi.org/10.18720/MPM.3222017_15.
[33] ASTM. Standard Terminology of Appearance, ASTM International West, Conshohocken, PA, 2017, pp. 1–25, https://doi.org/10.1520/E0284-17.
[34] E.E. Bell, Optical Constants and their Measurement, in: L. Genzel (Ed.), Light and Matter Ia / Licht Und Materie Ia, Springer, Berlin Heidelberg, Berlin, Heidelberg, 1967, pp. 1–58, https://doi.org/10.1007/978-3-642-46074-6_1.
[35] J.R. Frisvad, S.A. Jensen, J.S. Madsen, A. Correia, L. Yang, S.K.S. Gregersen, Y. Meuret, P.E. Hansen, Survey of models for acquiring the optical properties of translucent materials, in: Comput. Graph, Forum, Wiley Online Library, 2020, pp. 729–755, https://doi.org/10.1111/cgf.14023.

Ali Payami Golhin received his PhD in Engineering as a Marie Skłodowska-Curie fellow at NTNU - Norwegian University of Science and Technology. His research focuses on the study of the optical properties of structured surfaces. He has a research background in additive manufacturing, optical characterization, tribology, and materials engineering..

Are Strandlie is a Professor of Physics at NTNU - Norwegian University of Science and Technology. His main research interests are data analysis methods for high-energy physics experiments and numerical methods for material physics. Recently, an increasing interest has emerged within cross-disciplinary topics, such as the link between appearance and material properties.